RSC Advances

PAPER

View Article Online
View Journal | View Issue

Cite this: *RSC Adv.*, 2017, **7**, 41105

One-dimensional Cr-doped NiO nanostructures serving as a highly sensitive gas sensor for trace xylene detection

Changhao Feng, *[ab] Xueying Kou,[c] Xiaofeng Liao,[ab] Yanfeng Sun*[c] and Geyu Lu[c]

Received 11th June 2017
Accepted 8th August 2017

DOI: 10.1039/c7ra06517e

rsc.li/rsc-advances

A highly sensitive xylene sensor based on Cr-doped NiO nanotubes was presented, which was prepared using an electrospinning process. The responses of the sensors were investigated using a static system. We found that the sensors based on the Cr-doped NiO nanotubes exhibited a high response towards 50 ppm xylene, with a response of about 88, which was about 63 times higher than that of pure NiO nanotubes. The results obtained for the sensing properties indicate that the gas sensors based on Cr-doped NiO nanotubes are promising for monitoring air-quality and environmental pollution.

1. Introduction

Xylene is widely used in the field of building, in adhesives, paints, and as an antiseptic.[1–4] However, xylene causes great damage to human health, and it was ascribed as the main reason for sick-house syndrome, eye irritation, headache and fatigue.[5–7] The occupational safety and health administration (OSHA) suggest the permissible exposure limits for xylene is 100 ppm in an 8 hour period.[8] Therefore, detection of xylene is important for personal safety and environmental sustainability. Although some equipment such as gas chromatography-mass spectrometry and fluorescence spectroscopy can be used to measure the concentration of xylene,[9,10] these analyses requiring expensive and complex equipment aren't suitable for *in situ* monitoring. Thus, there is a strong demand for simple and portable xylene sensors with good sensing properties.

In recent years, gas sensors based on semiconductors have attracted significant attention for harmful and explosive gas detection.[11–14] Nickel oxide (NiO) is a kind of p-type semiconductor, which is widely used in the field of gas sensing.[12,15,16] In recent years, some approaches have been studied to enhance the gas sensing performance of NiO.[12,17,18] Among these methods, many researchers have confirmed that doping aliovalent metal oxides is a promising approach to improve gas sensing performance[19–24] and we have found that NiO nanotubes doped with W can enhance the gas sensing properties towards xylene and methanol, which has a response of about 8.74 to 200 ppm xylene.[25] Chromium oxide (Cr_2O_3) is a kind of p-type semiconductor, which is widely used as a dopant to enhance the response of gas sensors. For example, N. Al-Hardan doped Cr into ZnO films[26] and the sensitivity of the sensors towards oxygen was significantly enhanced. B. Lyson-Sypien synthesized Cr doped TiO_2 nanopowders using a flame spray method and the response towards H_2 was greatly enhanced using this method.[27] However, most of the reports are focused on the gas sensing properties of NiO or Cr_2O_3 and little attention has been given to the xylene-sensing properties of Cr-doped NiO with a 1D nanostructure.

To the best of our knowledge, there have been few reports on the gas sensing properties of Cr-doped NiO one-dimensional nanostructures. So in this work we synthesized Cr-doped NiO nanotubes and their gas sensing characteristics were investigated. These results indicate Cr doped NiO nanotubes with a molar ratio of Cr^{3+} : Ni^{2+} = 3 : 100, show outstanding sensing properties towards xylene. In addition, the effect of Cr doping was investigated and a possible mechanism was proposed.

2. Experimental details

2.1 Preparation of pure and Cr-doped NiO nanofibers

All chemicals were of analytical grade and used without further purification. Chromic nitrate ($Cr(NO_3)_3 \cdot 9H_2O$), polyvinyl pyrrolidone (PVP, K90) and *N*,*N*-dimethylformamide (DMF) were obtained from Sinopharm-Aldrich, USA. Nickel chloride ($NiCl_2$) and ethanol (C_2H_5OH) were purchased from Beijing Chemicals, China. The morphology of the samples was investigated using field emission scanning electron microscopy (FE-SEM; JEOL JSM-7500F) and transmission electron microscopy (TEM; JEOL JEM-3010). An X-ray diffractometer (Rigaku TTRIII) was used to analyze the phase and crystallinity of the nanomaterials. Energy-dispersive X-ray spectroscopy (EDS) and selected area electron diffraction (SAED) were performed using a TEM attachment.

[a]*College of Electronic and Information Engineering, Southwest University, Chongqing 400715, China. E-mail: fengchanghao@qq.com*

[b]*Chongqing Key Laboratory of Nonlinear Circuits and Intelligent Information Processing, Chongqing 400715, China*

[c]*State Key Laboratory on Integrated Optoelectronics, College of Electronic Science and Engineering, Jilin University, Changchun 130012, China. E-mail: syf@jlu.edu.cn*

The pure and Cr-doped NiO nanotubes (the molar ratio of Cr^{3+} to Ni^{2+} are 0 : 100, 1 : 100, 3 : 100 and 5 : 100) were synthesized using an electrospinning process and labeled as S1, S2, S3 and S4, respectively. In a typical synthesis process, 2 mmol of $NiCl_2$ and a certain amount of $Cr(NO_3)_3 \cdot 9H_2O$ (0.02, 0.06 and 0.1 mmol) were dissolved in 9 mL of DMF and 1 mL of ethanol, and stirred for 1 h at 50 °C. Then, 1 g of PVP was added and stirred at 50 °C, until a viscous precursor solution was completely formed and the precursor solution was placed into the electrospinning installation. The electrospinning installation is described in our previous works;[10] the inner diameter of the spinneret was 1.01 mm, the voltage between the spinneret and collector was 10–13 kV and the distance between the spinneret and collector was 10 cm. The flow rate of the precursor solution was fixed at 0.3 mL h^{-1} using a KD Scientific syringe pump. After the electrospinning experiment, the precursor nanofibers were calcined at 500 °C for 3 h in the air at a heating rate of 1 °C min^{-1} to completely decompose the PVP.

2.2 Fabrication and measurement of the gas sensor

Fig. 1(a) shows the photographs of the substrate. There are two L golden electrodes on the front-side and a ruthenium oxide (RuO_2) micro-heater on the back-side, which were made using a screen printing technique. The micro-heater was connected with Pt wire and the operating temperature was controlled by adjusting the current passing through the micro-heater. Fig. 1(b) shows the photographs of the gas sensor; the Cr-doped NiO nanotubes were mildly pressed on the substrate using a hot press machine (HS-XX40, Hesen Inc., China) at 120 °C for 5 min. By doing this, the sensing materials form a good contact with the electrodes. The temperature was distributed uniformity on the substrate, as shown in Fig. 1(c). The emissivity value of the temperature sensor (T250, FLIR Systems Inc., USA) was fixed at 0.9 and power consumptions of 102.1, 116.9, 129.8, 150.5, 165 and 188.5 mW were used to heat the substrates to 250, 275, 300, 325, 350 and 375 °C, respectively.

The gas sensing properties were measured using a static testing system, as shown in Fig. 2. Under the same conditions (relative humidity: 25–35% and temperature: 20–25 °C), the gas sensing properties of the nanotubes were tested. The response of the gas sensor (R) was defined as the ratio of resistance in air

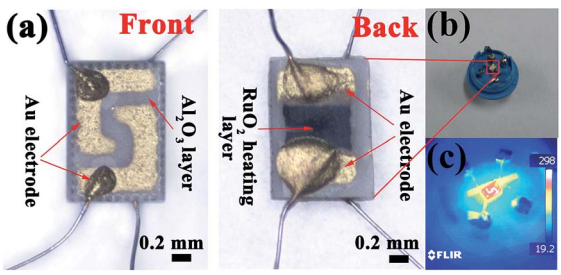

Fig. 1 (a) A schematic structure of the alumina substrate. (b) The photographs of the gas sensor. (c) The temperature distribution of the gas sensors.

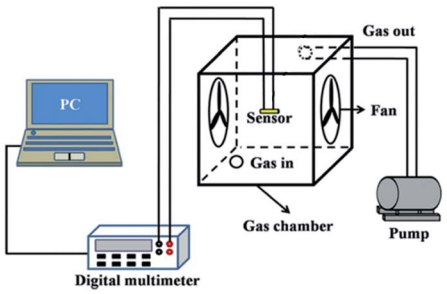

Fig. 2 The static gas-sensing characterization system.

(R_a) to that in the tested gas (R_g). The response time was defined as the time required by the sensor to attain 90% of its saturation resistance value after being exposed to the target gas. The recovery time is characterized as the time lag to reach its baseline value (90%) after the target gas was withdrawn.

3. Results and discussion

3.1 Characterization

Fig. 3 is the SEM images of the pure NiO and Cr-doped NiO nanotubes after calcination. These nanotubes display porous structures, which are beneficial for the diffusion of target gas and may enhance the response of the gas sensor. As shown in the insets of Fig. 3, the nanotubes are composed of many small nanoparticles. In addition, Fig. 3(b)–(d) are the FESEM images of the Cr-doped NiO nanotubes (S2, S3 and S4). When compared to the S1 nanotubes, the morphology of S4 was changed significantly, the S1 nanotubes are porous while the S4 nanotubes become tighter. This is because Cr doping impedes the growth of the nanoparticles, which was also confirmed by the XRD results. What's more, there are some large nanoparticles on the backbones of the nanotubes, when the amount of Cr doping was increased to 5 mol%. We think this may be caused by the mismatch in the NiO lattice. Further study and systematic experiments are needed for a deeper understanding of this.

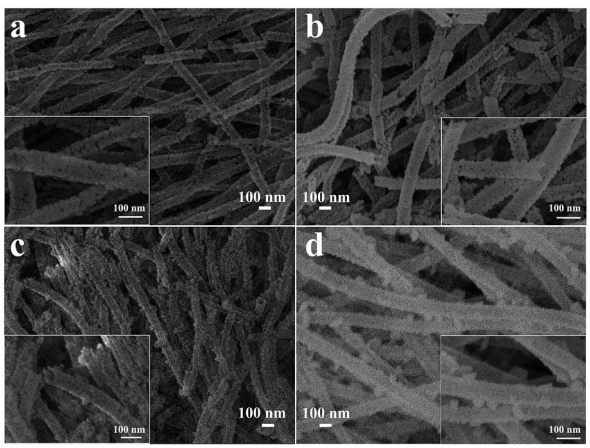

Fig. 3 The FESEM images of (a) S1, (b) S2, (c) S3 and (d) S4, the insets are the high-magnification images.

TEM was employed to further study the internal structure of the NiO nanotubes. Fig. 4(a) and (b) are the TEM images of the S4 sample and it obviously confirmed this one-dimensional structure was nanotubes. The inset of Fig. 4(a) is the SAED pattern obtained from the marked circle, which demonstrates the backbones are polycrystalline. Fig. 4(b) shows the HRTEM images and the lattice fringes can be clearly observed and the lattice spacing was 0.209 nm corresponding to the (100) planes of NiO. Fig. 4(c)–(g) are the EDS results, which clearly show the spatial distribution of the elements Ni, Cr and O. As shown in Fig. 4(e), Cr was uniformly distributed in the nanotubes and the peaks for Cr can be clearly seen in Fig. 4(g). Therefore, the EDS results demonstrate that Cr can enter the NiO lattice using this method.

Fig. 5 presents the XRD patterns of the S1, S2, S3 and S4 nanotubes. As Fig. 5(a) shows, the diffraction peaks can be readily indexed to a cubic NiO phase, which is in a good agreement with JCPDS: 47-1049. Because the doping amount is small, there are no phases corresponding to the chromic compound observed in the XRD patterns. The diffraction peaks of nanotubes S1 to S4 become broader upon increasing the amount of Cr, which demonstrates that the grain size of the samples decreases. The average crystal size of S1, S2, S3 and S4 were calculated using the Debye–Scherrer formula. The average crystal sizes of S1, S2, S3 and S4 are about 19.6 nm, 16.0 nm, 12.9 nm and 12.0 nm, respectively. What's more, as the radius of Cr^{3+} and Ni^{2+} are 0.0615 nm and 0.069 nm at a coordination number (CN) of 6, the diffraction peaks shift to the right as the Cr doping amount increased. There is a 0.06° right shift in the (1 1 1) and (2 0 0) diffraction peaks of the S4 nanotubes when compared with S1, as shown in Fig. 5(b). The results indicate that Cr^{3+} can enter the NiO lattice easily.

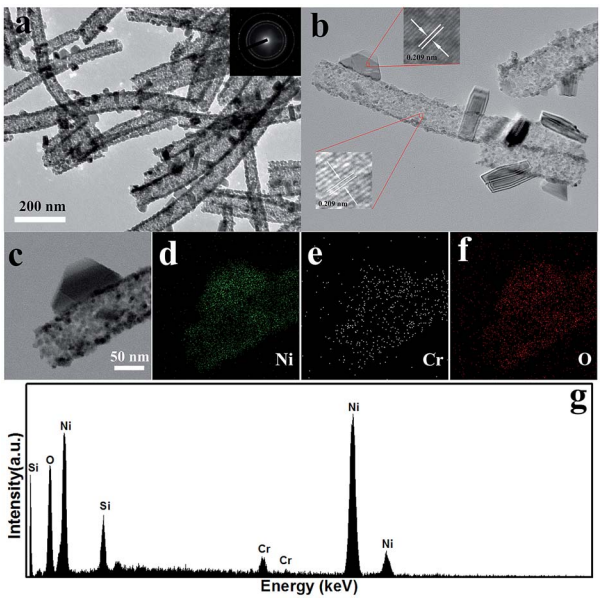

Fig. 4 (a) The TEM images of the S4 nanotubes. The insets are the selected area electron diffraction (SAED) patterns and (b) is the TEM image. The inset is the HRTEM of the selected areas. (c)–(f) The EDS elemental maps and (g) spots pattern of Cr, Ni and O.

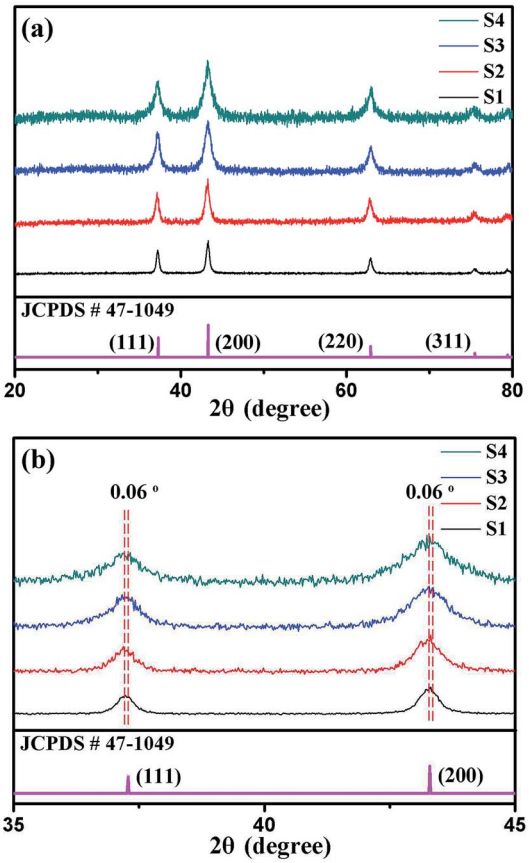

Fig. 5 (a) The XRD patterns of Cr–NiO nanotubes with different molar ratios. (b) A comparison of the (111) and (200) peaks obtained from the XRD patterns.

3.2 Xylene sensing properties

Gas sensors based on the Cr-doped NiO nanotubes were fabricated and a series of gas sensing measurements were carried out. In order to determine the optimum operating temperatures of the sensors, the responses to 50 ppm xylene were tested as a function of the operating temperature, as shown in Fig. 6(a). It clearly shows that the responses of the sensors to xylene varied with temperature and exhibited an 'increase-maximum-decrease' tendency. For sensor S3, there is not enough energy to make the oxygen species effectively react with the xylene vapor at low temperature. At 325 °C, all the oxygen species have the required energy to react with the target gas, so both the higher reaction activity and the conversion of the surface absorbed oxygen species ($O_{2(gas)} \rightarrow O_{2(ads)} \rightarrow O_2^- \rightarrow 2O^-$) contributed to the higher response. However, when the temperature was above 325 °C, the response reduced because of the amount of adsorbed gas molecules was insufficient to react with the oxygen species. Therefore, 325 °C was selected as the operating temperature of sensor S3 in following gas testing process. Similar behavior can be observed in the case of sensors S1, S2 and S4. However, their maximal responses appeared at different temperatures, sensor S1 has a maximum gas response at 325 °C, while sensors S2 and S4 have maximum gas responses at 300 °C and 350 °C, respectively. What's more, sensor S3 shows the

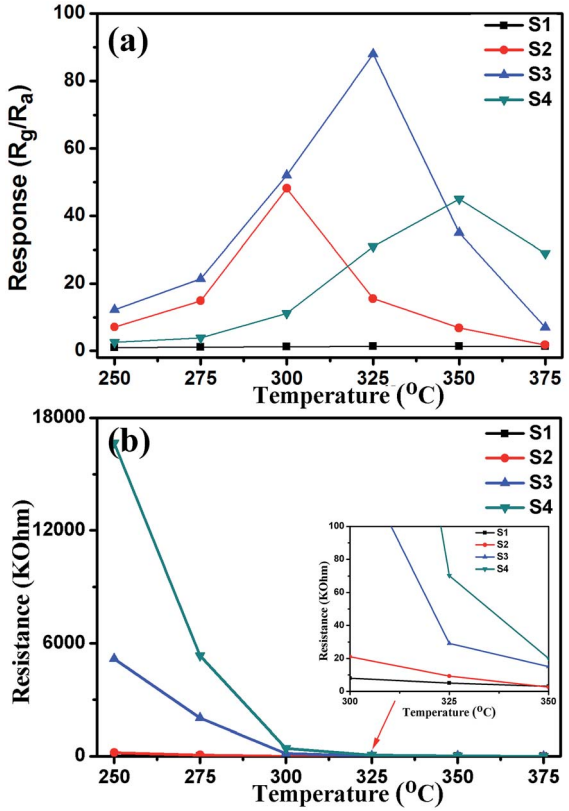

Fig. 6 (a) The response of nanotubes S1, S2, S3 and S4 to 50 ppm xylene as a function of the operating temperature. (b) The resistance of the samples in air as a function of the operating temperature.

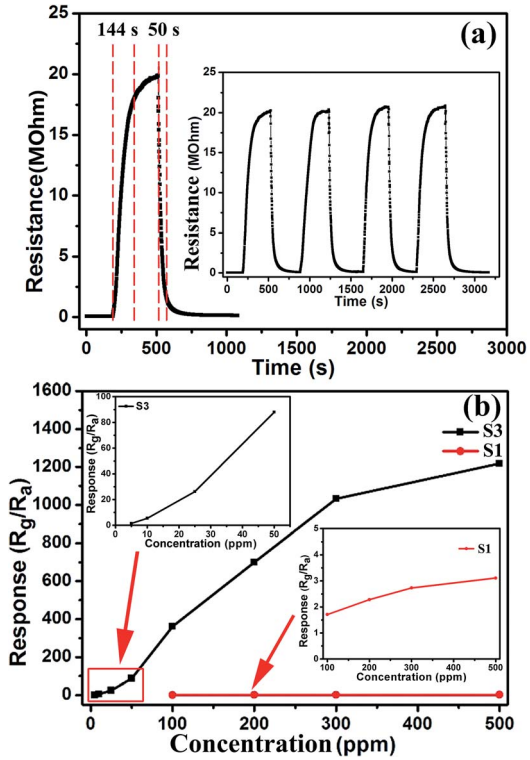

Fig. 7 (a) The response of the S3 nanotubes towards 200 ppm xylene. The inset displays four periods of the response curve. (b) The response of nanotubes S1 and S3 towards xylene at different concentrations; the inset on the left is the response of the S3 nanotubes towards xylene at concentrations between 5–50 ppm. The inset on the right is the response of the S1 nanotubes towards xylene at concentrations between 100–500 ppm.

highest response towards 50 ppm xylene with a maximum response of 88, which is about 63 times higher than sensor S1. As shown in Fig. 6(b), the resistance in air (R_a) was increased as the doping amount increased and the R_a of S1, S2, S3 and S4 are 5.1, 9.3, 29.1 and 70.2 kΩ, respectively, at 325 °C.

Fig. 7(a) is the dynamic characteristics of the S3 sensor to 200 ppm xylene; the response and recovery time are ~144 s and 50 s, rspectivley. There are four reversible response curves in the inset of Fig. 7(a). These results indicate the gas sensors based on Cr doped NiO displayed a fast response, recovery and good repeatability. Fig. 7(b) reveals the response as a function of the xylene concentration. The concentration of xylene was varied from 5 to 500 ppm and the responses of sensors S1 and S3 both increased upon increasing the xylene concentration and the response of the S3 sensor was obviously higher than S1. For sensors S3, the response was 1219 for 500 ppm xylene and the detection limit was 5 ppm with a response of 1.42. While the response of sensor S1 to 500 ppm xylene was 3.11 and the detection limit was 100 ppm with a response of 1.71. Evidently, doping with Cr can effectively enhance the response towards xylene.

Fig. 8 shows the selectivity of sensors S1 and S3, which were evaluated by exposing to six kinds of gases with a concentration of 200 ppm at 325 °C, including xylene, ethanol, acetone, methanol, formaldehyde and benzene. It can be seen that sensor S3 displayed an ultra-enhanced response to most of the test gases when compared with sensor S1. In addition, the

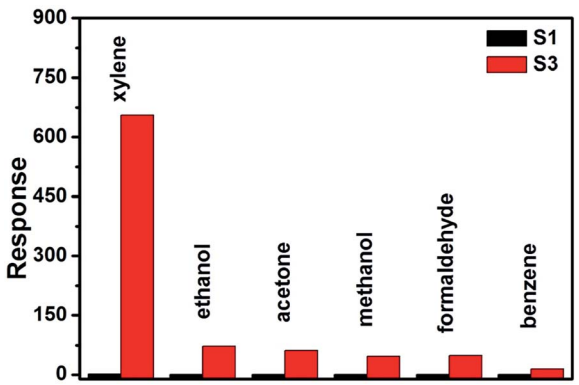

Fig. 8 A comparison of the response of nanotubes S1 and S3 towards different gases at 200 ppm.

response towards xylene was remarkably higher than the other gases with a response of 656, while the responses to ethanol, acetone, methanol, formaldehyde and benzene were much lower. Therefore, it was revealed that the Cr-doped NiO nanotubes showed an excellent selectivity towards xylene.

The long-term stability is a crucial parameter for evaluating the gas sensing performance in practical applications. The response as a function of the number of testing days was

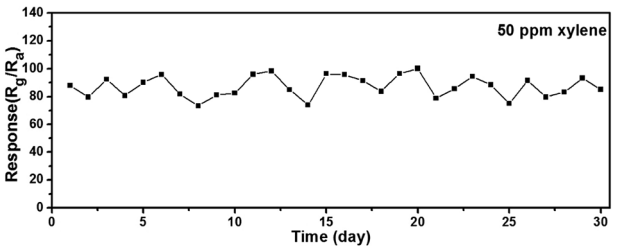

Fig. 9 The long-term stability of sensor S3 at 325 °C.

measured and shown in Fig. 9. The responses of sensor S3 to 50 ppm xylene were tested under the same temperature and humidity conditions over 30 days. Even though the response changed every day, we can see that the response values are floating around 88, which shows its good stability.

A widely accepted sensing mechanism for this type of gas sensor is based on the resistance changes during the adsorption and desorption processes.[2] When the pure NiO nanotubes or Cr-doped NiO nanotubes are exposed to an air atmosphere, the adsorbed oxygen molecules will ionize and attract holes to the surfaces and the hole accumulation layer (HAL) will lead become thick, which will result in a decrease in the resistance. On exposure to the reducing gas, such as xylene, the testing gases will be oxidized by the ionized oxygen and release electrons,[10] which will decrease the concentration of holes and the HAL will become thinner and the resistance will increase. What's more, the highly enhanced gas sensing properties of the Cr-doped NiO nanotubes are likely to be explained as follows. According to previous research by Hyo-Joong Kim,[11] the response of p-type semiconductors can be written as follows:

$$S = \frac{R_g}{R_a} = \frac{p_a}{p_g} = \frac{p_a}{p_a - \Delta p} = \frac{\Delta p}{(p_a - \Delta p)} + 1 \quad (1)$$

where R_a and R_g are the resistance of the nanotubes in air and the target gas, respectively, p_a and p_g are the hole concentrations in air and the target gas, respectively and $\Delta p = p_a - p_g$ is the variation of hole concentration when exposed to the target gas. When Cr was doped into the NiO lattice, the substitution of Cr^{3+} at the Ni^{2+} site can be compensated by the electronic compensation mechanism and the generation of electrons will decrease the concentration of holes. So the p_a of the Cr-doped NiO nanotubes was lower than that of pure NiO and the responses of sensors S2 and S3 are enhanced. This can be proved by the R_a of S1, S2 and S3, which are 5.1, 9.3 and 29.1 kΩ at 325 °C, with the response of S1, S2 and S3 to 200 ppm xylene being 1.3, 15.5 and 88, respectively. However, when the molar ratio of Cr^{3+}/Ni^{2+} was increased to 5%, we believe that the degradation of gas sensing characteristics was due to the compact structure. When compare to the S3 nanotubes, the S4 nanotubes become tighter, so the gas sensing efficiency will be reduced. For this reason, the response of sensor S4 was lower than sensor S3.

4. Conclusions

In summary, a series of Cr doped-NiO nanotubes have been synthesized *via* a simple and facile technique, and their gas sensing properties were investigated. The gas sensors based on the S3 nanotubes demonstrated good selectivity, repeatability and long term stability at 325 °C. The method of modulating the concentration of hole provides a new and promising strategy to design high performance xylene sensors. The good xylene sensing characteristics indicate that the presented sensors based on Cr-doped NiO nanotubes are promising for xylene sensing and can used for air-quality and environmental monitoring.

Conflicts of interest

There are no conflicts to declare.

Acknowledgements

This work is supported by the Fundamental Research Funds for the Central Universities (Grant No. XDJK2017C074, SWU116059 and SWU116013), China Postdoctoral Science Foundation (Grant No. 2016M602631 and 2017M610583) and National Nature Science Foundation of China (Grant No. 61134010, 61304242, 61703348, 61327804, 61377058 and 61374218).

Notes and references

1 J. Hue, M. Dupoy, T. Bordy, R. Rousier, S. Vignoud, B. Schaerer, T. H. Tran-Thi, C. Rivron, L. Mugherli and P. Karpe, *Sens. Actuators, B*, 2013, **189**, 194–198.
2 J. H. Lee, *Sens. Actuators, B*, 2009, **140**, 319–336.
3 A. K. Srivastava, *Sens. Actuators, B*, 2003, **96**, 24–37.
4 Y. S. Kim, S. C. Ha, H. Yang and Y. T. Kim, *Sens. Actuators, B*, 2007, **122**, 211–218.
5 Y. Li, Y. Cao, D. Jia, Y. Wang and J. Xie, *Sens. Actuators, B*, 2014, **198**, 360–365.
6 Y. Cao, P. Hu, W. Pan, Y. Huang and D. Jia, *Sens. Actuators, B*, 2008, **134**, 462–466.
7 K. Niaz, H. Bahadar, F. Maqbool and M. Abdollahi, *EXCLI J.*, 2015, **14**, 1167–1186.
8 H. J. Kim, J. W. Yoon, K. I. Choi, H. W. Jang, A. Umarcd and J. H. Lee, *Nanoscale*, 2013, **5**, 7066–7073.
9 K. W. Kao, M. C. Hsu, Y. H. Chang, S. Gwo and J. A. Yeh, *Sensors*, 2012, **12**, 7157–7168.
10 C. Feng, X. Li, C. Wang, Y. Sun and G. Lu, *RSC Adv.*, 2014, **4**, 47549–47555.
11 H. Kim, K. Choi, K. Kim, C. W. Na and J. H. Lee, *Sens. Actuators, B*, 2012, **171–172**, 1029–1037.
12 P. Rai, J. Yoon, H. Jeong, S. Hwang, C. Kwaka and J. H. Lee, *Nanoscale*, 2014, **6**, 8292–8299.
13 N. Yamazoe, G. Sakai and K. Shimanoe, *Catal. Surv. Asia*, 2003, **7**, 63–75.
14 J. Tamaki, *Sens. Lett.*, 2005, **3**, 89–98.
15 J. A. Dirksen, K. Duval and T. A. Ring, *Sens. Actuators, B*, 2001, **80**, 106–115.
16 P. V. Tong, N. D. Hoa, N. V. Duy, V. V. Quang, N. T. Lam and N. V. Hieu, *Int. J. Hydrogen Energy*, 2013, **38**, 12090–12100.
17 R. K. Jamal, K. A. Aadim, Q. G. Al-Zaidi and I. N. Taaban, *Photonic Sens.*, 2015, **5**, 235–240.

18 Y. Liu, G. Li, R. Mi, C. Deng and P. Gao, *Sens. Actuators, B*, 2014, **191**, 537–544.
19 Y. Zhang and W. Zeng, *Mater. Lett.*, 2017, **195**, 217.
20 M. Tonezzer, T. T. L. Dang, Q. H. Tran, V. H. Nguyen and S. Iannotta, *Int. J. Hydrogen Energy*, 2017, **42**, 740.
21 M. K. Khalaf, R. H. Mutlak, A. I. Khudiar and Q. G. Hial, *Phys. B*, 2017, **514**, 78.
22 U. Cindemir, M. Trawka, J. Smulko, C. Granqvist, L. Österlund and G. A. Niklasson, *Sens. Actuators, B*, 2017, **242**, 132.
23 Y. Lu, Y. H. Ma, S. Y. Ma, W. X. Jin, S. H. Yan, X. L. Xu and Q. Chen, *Mater. Lett.*, 2017, **190**, 252.
24 M. Tonezzer, T. T. L. Dang, Q. H. Tran and S. Iannotta, *Sens. Actuators, B*, 2016, **236**, 1011.
25 C. Feng, X. Li, J. Ma, Y. Sun, C. Wang, P. Sun, J. Zheng and G. Lu, *Sens. Actuators, B*, 2015, **209**, 622–629.
26 N. Al-Hardan, M. J. Abdullah, A. Abdul Aziz and H. Ahmad, *Appl. Surf. Sci.*, 2010, **11**, 3468–3471.
27 B. Lyson-Sypien, A. Czapla, M. Lubecka, P. Gwizdz and K. Schneider, *Sens. Actuators, B*, 2012, **175**, 163–172.